PHYSICAL REVIEW D **78,** 063540 (2008)

Direct/indirect detection signatures of nonthermally produced dark matter

Minoru Nagai[1] and Kazunori Nakayama[2]

[1]*Theory Group, KEK, Oho 1-1, Tsukuba, Ibaraki 305-0801, Japan*

[2]*Institute for Cosmic Ray Research, University of Tokyo, Kashiwa, Chiba 277-8582, Japan*

(Received 23 July 2008; published 29 September 2008)

We study direct and indirect detection possibilities of neutralino dark matter produced nonthermally by, e.g., the decay of long-lived particles, as is easily implemented in the case of anomaly or mirage-mediation models. In this scenario, large self-annihilation cross sections are required to account for the present dark matter abundance, and it leads to significant enhancement of the gamma-ray signature from the galactic center and the positron flux from the dark matter annihilation. It is found that GLAST and PAMELA will find the signal or give tight constraints on such nonthermal production scenarios of neutralino dark matter.

DOI: 10.1103/PhysRevD.78.063540 PACS numbers: 98.80.Cq, 14.80.Ly, 95.35.+d

I. INTRODUCTION

While there is a lot of cosmological evidence of dark matter in the Universe [1,2], its detailed properties remain largely undetermined. Requirements for the dark matter particle are the following. (1) It reproduces the present matter density of the Universe. In terms of the density parameter, $\Omega_m h^2 \sim 0.11$ must be satisfied where $h(\sim 0.70)$ is the Hubble parameter in units of 100 km/s/Mpc [3]. (2) It is electrically neutral. (3) It is cold, which means that its free-streaming (FS) length ($\lambda_{\rm FS}$) is not so long as to seed the structure formation satisfactory, and this requires $\lambda_{\rm FS} \lesssim 1$ Mpc.

In fact, many candidates of dark matter are proposed in the framework of physics beyond the standard model. In particular, supersymmetry (SUSY) provides interesting candidates. If R parity is conserved, the lightest SUSY particle (LSP) becomes stable and contributes present matter density of the Universe. Among SUSY particles, the gravitino and (lightest) neutralino are possible candidates of the LSP dark matter. From the viewpoint of detection possibility, the gravitino dark matter is undesirable because its interaction strength with ordinary matter is Planck suppressed.[1] In the following, our focus is the neutralino dark matter, which may have distinct signatures of direct and/or indirect detection.

Usually neutralinos are assumed to be produced thermally as in the following scenario [1,5]. In the early universe with temperature $T \gtrsim 1$ TeV, SUSY particles, including neutralinos, are thermalized and their number density is given by $\sim T^3$. As the temperature decreases, their thermal abundance receives the Boltzmann suppression factor and eventually they decouple from the thermal bath at the freeze-out temperature $T_f \sim m_{\rm L}/20$, where $m_{\rm L}$ denotes the LSP mass. After that, the number density of the LSP per comoving volume remains constant until now and hence contributes as dark matter of the Universe. The resultant abundance of the LSP is estimated as

$$Y_{\rm L} \equiv \frac{n_{\rm L}}{s} \sim \frac{1}{T_f M_P \langle \sigma v \rangle}, \tag{1}$$

where $\langle \sigma v \rangle$ denotes the annihilation cross section of the LSP and M_P is the reduced Planck scale ($= 2.4 \times 10^{18}$ GeV).

However, such a thermal relic scenario does not always hold in realistic SUSY models. For example, there often exists a Polonyi or moduli field in order to break SUSY and gives rise to the correct order of gaugino masses. Those singlet scalar fields generally have a long lifetime and decay after freeze-out of the LSP, yielding a substantial amount of LSPs. Actually Polonyi/moduli dominate the Universe before they decay, and hence reheat the Universe again with a very low reheating temperature of $O(1)$ MeV–$O(1)$ GeV depending on their masses [6,7]. In this case a large amount of LSPs are produced nonthermally by the Polonyi/modulus decay, and hence a large annihilation cross section is needed to account for the present dark matter abundance. Therefore, taking into account the nonthermal production mechanism may significantly change the properties of the LSP and its direct/indirect detection signatures.

Thus, in this paper we study direct/indirect detection signatures of nonthermally produced neutralino dark matter. As for direct detection, there are some ongoing and planned projects devoted to detect scattering signals of the LSP with nucleons such as CDMS [8] and XENON [9]. As for indirect detection, many possible ways are proposed. First, neutralinos accumulated in the Galactic center annihilate each other and produce line and continuum gamma rays. Such gamma-ray signals can be searched by satellite experiments (GLAST [10]) or ground-based Cerenkov telescopes (HESS [11], MAGIC [12], CTA [13]).

Second, antimatter such as positrons or antiprotons are produced by the annihilation of the neutralinos. Since these particles are diffused by galactic magnetic fields during

[1]Recently, it was pointed out that the detection of inflationary gravitational wave background can help the situation [4].

their propagation to the Earth, we need to solve its propagation in a diffusion model to discuss their flux on the Earth [14]. Fortunately, the positron flux is less sensitive to the precise diffusion model since magnetic fields easily dissipate their energy through the propagation and positrons come only from near the Earth. These antimatter signals can be detected with PAMELA [15] and AMS-02 [16].

Third, neutralinos trapped in the Sun annihilate and produce high-energy neutrinos. Super-Kamiokande [17], AMANDA [18], IceCube [19], and the planned KM3NeT [20] experiments search high-energy muon signals, which arise from high-energy neutrino interaction with Earth matter. We investigate characteristic signals of nonthermal neutralino dark matter on these experiments.

For the sake of concreteness, we stick to two SUSY breaking models: the minimal anomaly-mediated SUSY breaking model [21] and mirage-mediation model [22]. The former model predicts the winolike neutralino LSP in broad parameter regions. Since the winolike neutralino with a mass of $\mathcal{O}(100)$ GeV has annihilation cross sections that are too large, its thermal abundance becomes too small to account for the present dark matter abundance. Hence, we need to consider some nonthermal production processes of the neutralino dark matter. The latter model contains a heavy modulus field and nonthermal production of the neutralino dark matter is expected naturally. As we will see later, the large annihilation cross section of the neutralino dark matter is a general feature of the nonthermal production scenario, and hence our results are less sensitive to the model construction.

A similar subject was studied in Ref. [23], where it was pointed out that the large annihilation cross section of the neutralino yields enhancement of the antimatter signals. We emphasize that such an enhancement is a rather generic feature when considering the nonthermal production scenario of the dark matter, and its detection may be directly related to the early universe cosmology, in particular, the existence of late-decaying particles and their decay temperature. Also, we have performed more detailed parameter analyses both in the anomaly-mediated SUSY breaking and mirage-mediation models, including the gamma-ray signature as well as antimatter searches.

This paper is organized as follows. In Sec. II, we review some nonthermal production mechanisms of the neutralino dark matter. The minimal anomaly-mediated SUSY breaking model and the mirage-mediation mode are taken as examples. In Sec. III, detection possibilities of nonthermal dark matter are discussed. These include direct detection using recoil of nuclei by the neutralino, gamma-ray flux from the neutralino annihilation at the Galactic center, positron flux from the annihilation near the Earth, and high-energy neutrino flux from the annihilation in the Sun. Section IV is devoted to our conclusions.

For calculating these direct/indirect detection rates, we have utilized DarkSUSY code [24].

II. NONTHERMAL PRODUCTION OF NEUTRALINO DARK MATTER

The LSP neutralino is often referred to as a promising candidate of the dark matter of the Universe. Although the standard thermal relic scenario is often assumed, the production processes of the neutralino are not limited to it in general. In particular, nonthermal production processes may be relevant for estimating the present dark matter abundance. Actually, we often encounter the cosmological scenarios which include long-lived matter. If the long-lived matter has a non-negligible fraction of the total energy density at the time of its decay, neutralinos emitted by its decay processes may amount to a significant contribution to the dark matter abundance [25]. Here we present examples of such late-decaying matter.

(1) Gravitino: The gravitino is the superpartner of the graviton and its interaction strength is suppressed by the Planck scale or SUSY breaking scale. Gravitinos are efficiently produced in the early universe thermally [26] or nonthermally by the next-to-lightest supersymmetric particle [27,28] and/or inflaton decay [29]. Its thermal abundance is given by

$$\left(\frac{\rho_{3/2}}{s}\right)^{(\mathrm{TP})} \simeq 1.9\times 10^{-7}\ \mathrm{GeV}\left(\frac{m_{3/2}}{100\ \mathrm{TeV}}\right)\left(\frac{T_R}{10^{10}\ \mathrm{GeV}}\right) \times\left[1+0.045\ln\left(\frac{T_R}{10^{10}\ \mathrm{GeV}}\right)\right] \times\left[1-0.028\ln\left(\frac{T_R}{10^{10}\ \mathrm{GeV}}\right)\right], \quad (2)$$

for a heavy gravitino where TP denotes a thermally produced one and $m_{3/2}$ is the gravitino mass and T_R is the reheating temperature of the Universe defined as $T_R = (10/\pi^2 g_*)^{1/4}\sqrt{\Gamma_{\mathrm{inf}} M_P}$ with the total decay rate of the inflaton Γ_{inf}. If the gravitino is unstable, it decays later at the epoch after the freeze-out of the LSP. In the case of the heavy gravitino ($m_{3/2} \gtrsim 100$ TeV) as is realized in anomaly-mediated SUSY breaking, it decays well before the big bang nucleosynthesis (BBN) begins without affecting the success of BBN, and produces LSP nonthermally. The lifetime of the gravitino is estimated as

$$\tau_{3/2} \simeq \left(\frac{193}{384\pi}\frac{m_{3/2}^3}{M_P^2}\right)^{-1} \simeq 2.4\times 10^{-2}\ \mathrm{sec}\left(\frac{100\ \mathrm{TeV}}{m_{3/2}}\right)^3, \quad (3)$$

if the gravitino is the heaviest among minimal supersymmetric standard model (MSSM) particles. Depending on the reheating temperature, the abundance of nonthermally produced LSPs by the gravitino decay can exceed that of thermally produced ones.

(2) Polonyi field: A Polonyi field is a singlet scalar responsible for SUSY breaking. A Polonyi field is always required in gravity-mediation models in order to generate sizable gaugino masses. However, generically Polonyi has

the mass (m_χ) of order of the gravitino ($m_{3/2}$) and its interaction is Planck-suppressed. Thus, decay of the coherent oscillation of the Polonyi causes cosmological disaster, unless Polonyi decays well before BBN or it is diluted by some additional entropy production processes. The Polonyi field begins to oscillate when the Hubble parameter become equal to the Polonyi mass, and its abundance is estimated as

$$\frac{\rho_\chi}{s} = \frac{1}{8} T_R \left(\frac{\chi_0}{M_P}\right)^2 \gamma \simeq 1 \times 10^5 \text{ GeV} \left(\frac{T_R}{10^6 \text{ GeV}}\right)\left(\frac{\chi_0}{M_P}\right)^2 \gamma, \tag{4}$$

where χ_0 is the initial amplitude of the Polonyi field. Here γ is defined as

$$\gamma = \begin{cases} 1 & (m_\chi > \Gamma_{\text{inf}}) \\ T_{\text{osc}}/T_R & (m_\chi < \Gamma_{\text{inf}}), \end{cases} \tag{5}$$

where $T_{\text{osc}} = (90/\pi^2 g_*)^{1/4}\sqrt{m_\chi M_P}$. If the Polonyi mass is larger than $\sim$100 TeV, it decays before BBN begins. The lifetime is estimated as

$$\tau_\chi \simeq \left(\frac{1}{4\pi}\frac{m_\chi^3}{M_P^2}\right)^{-1} \simeq 4.9 \times 10^{-2} \text{ sec} \left(\frac{100 \text{ TeV}}{m_\chi}\right)^3. \tag{6}$$

In general, the Polonyi field also decays into SUSY particles and their abundance may be bigger than the thermal relic one [6,7,30,31]. Thus we must take into account the abundance of the LSP arising from the Polonyi decay.

(3) Moduli: Modulus field is a scalar field appearing in the low energy effective theory of string theory when the extra dimensions are compactified. Properties and their cosmological effects are similar to those of the Polonyi [32]. In some particular models the modulus mass is related to the gravitino mass. For example, in the Kachru-Kallosh-Linde-Trivedi (KKLT) [33] setup described below, $m_\chi \sim 4\pi^2 m_{3/2}$ is obtained. In such a case, the decay temperature of the modulus can be as large as $\sim O(1)$ GeV [34], although gravitinos produced by the modulus decay may cause another cosmological difficulty [35,36].[2]

(4) Saxion: In the SUSY extension of the axion models, there exists an additional light scalar degree of freedom, which obtains a mass from the SUSY breaking effect, called saxion (σ) [38]. The saxion mass is naturally expected to be $\sim m_{3/2}$ and its interaction strength is suppressed by the Peccei-Quinn (PQ) scale $f_{\text{PQ}}(\sim 10^{10-12}$ GeV). Saxions are produced in the early universe via the coherent oscillation and their decay process affects cosmology [39–41]. Its coherent oscillation contribution is given by

$$\frac{\rho_\sigma}{s} = \frac{1}{8} T_R \left(\frac{\sigma_0}{M_P}\right)^2 \gamma \simeq 2 \times 10^{-8} \text{ GeV} \left(\frac{T_R}{10^6 \text{ GeV}}\right)\left(\frac{f_{\text{PQ}}}{10^{12} \text{ GeV}}\right)^2 \left(\frac{\sigma_0}{f_{\text{PQ}}}\right)^2 \gamma, \tag{7}$$

where σ_0 is initial amplitude of the saxion and γ is defined analogously to the Polonyi case. If we assume that the main decay mode is $\sigma \to 2g$, where g denotes the gluon, the lifetime is estimated as

$$\tau_\sigma = \left(\frac{\alpha_s^2}{32\pi^3}\frac{m_\sigma^3}{f_{\text{PQ}}^2}\right)^{-1} \simeq 4.7 \times 10^{-5} \text{ sec} \left(\frac{1 \text{ TeV}}{m_\sigma}\right)^3 \left(\frac{f_{\text{PQ}}}{10^{12} \text{ GeV}}\right)^2. \tag{8}$$

If the saxion is heavier than the LSP, decay modes into LSPs or SUSY particles become open and they give significant fractions of the relic LSP density [42]. Axino, which is the fermionic superpartner of the axion, may also produce a large amount of LSPs by its decay, if unstable [43,44].

(5) Q-Ball: Q-ball is a nontopological soliton whose stability is ensured by a global U(1) symmetry [45]. In SUSY, flat direction condensates (called the Affleck-Dine field) can develop to large field value during inflation and coherent motion of the Affleck-Dine (AD) field can create an observed amount of baryon asymmetry [46]. Through the dynamics of the AD field, fluctuation of the AD field develops if its potential is flatter than the quadratic one and then it fragments into solitonic objects, Q-balls [47,48]. Here the global U(1) charge required to stabilize the Q-ball configuration is a baryon number. Assuming that the AD field begins to oscillate at $H \sim m_\phi$ with amplitude ϕ_i, the Q-ball charge (Q) is estimated as [49][3]

$$Q = \gamma \left(\frac{\phi_i}{m_\phi}\right)^2 \times \begin{cases} \epsilon & (\epsilon > 0.01) \\ 0.01 & (\epsilon < 0.01), \end{cases} \tag{9}$$

where $\gamma \sim 6 \times 10^{-3}$ is a numerical constant and ϵ is called an ellipticity parameter, which is smaller than 1. In the case of AD baryogenesis using flat directions lifted by a non-renormalizable (NR) superpotential $W_{\text{NR}} \sim \phi^6/M^3$ with a cutoff scale M, we obtain $\phi_i \sim (m_\phi M^3)^{1/4}$. Thus the charge of the Q-ball becomes

$$Q \sim 7 \times 10^{20} \left(\frac{1 \text{ TeV}}{m_\phi}\right)^{3/2} \left(\frac{M}{M_P}\right)^{3/2}. \tag{10}$$

Once a Q-ball is formed, its lifetime is determined by the charge of the Q-ball [50],

[2] See, also, [37] for models of heavy moduli and their cosmological effects.

[3] Here we assume a gravity-mediation type Q-ball.

$$\tau_Q \simeq \frac{48\pi\kappa Q}{m_\phi} \simeq 9.9 \times 10^{-7}\ \text{sec}\left(\frac{\kappa}{10^{-2}}\right)\left(\frac{Q}{10^{21}}\right)\left(\frac{1\ \text{TeV}}{m_\phi}\right), \tag{11}$$

where m_ϕ denotes the mass of the AD field and κ is a model dependent constant which can take the value $\sim$1–10^{-4}. On the other hand, the abundance of the Q-ball is given by

$$\frac{\rho_Q}{s} = \frac{1}{8} T_R \left(\frac{\phi_i}{M_P}\right)^2 \gamma. \tag{12}$$

Thus, decay of the Q-balls yields significant amount of LSPs nonthermally [51,52], and they can even dominate the Universe before the decay [53]. Interestingly, this model can explain the present dark matter abundance and baryon asymmetry simultaneously by the Q-ball decay.

All the above models predict decay temperature of order 0.1–1 GeV typically, which is smaller than the freeze-out temperature of LSP. In this case, the nonthermally produced LSP abundance may exceed the thermal relic one. Thus, it is important to reconsider the abundance of the LSP produced by the decay of those long-lived matters. Hereafter, we collectively denote such a long-lived matter as χ. The following arguments do not depend on the detailed properties of χ once the decay temperature of χ is fixed.

Now let us write down the Boltzmann equations which govern the evolution of the number density of the LSP,

$$\dot{n}_{\rm L} + 3Hn_{\rm L} = -\langle\sigma v\rangle n_{\rm L}^2 + 2B_{\rm L}\Gamma_\chi n_\chi, \tag{13}$$

$$\dot{n}_\chi + 3Hn_\chi = -\Gamma_\chi n_\chi, \tag{14}$$

$$\dot{\rho}_r + 4H\rho_r = (m_\chi - 2B_{\rm L} m_{\rm L})\Gamma_\chi n_\chi + m_{\rm L}\langle\sigma v\rangle n_{\rm L}^2, \tag{15}$$

where $n_{\rm L}$ and n_χ denote the number density of the LSP and late-decaying particle, $\langle\sigma v\rangle$ denotes a thermally averaged annihilation cross section of the LSP,[4] ρ_r denotes the radiation energy density, $m_{\rm L}$ denotes the LSP mass, $B_{\rm L}$ denotes the branching fraction of the χ decay into LSP or SUSY particles, and H denotes the Hubble parameter. This set of equations is simplified for $t > 1/\Gamma_\chi$ after χ decays,

$$\dot{n}_{\rm L} + 3Hn_{\rm L} = -\langle\sigma v\rangle n_{\rm L}^2. \tag{16}$$

This equation can easily be solved and the resulting abundance of LSP is simply given by

$$Y_{\rm L}(T) = \left[\frac{1}{Y_{\rm L}(T_\chi)} + \sqrt{\frac{8\pi^2 g_*}{45}}\langle\sigma v\rangle M_P (T_\chi - T)\right]^{-1}, \tag{17}$$

where we have defined the number-to-entropy ratio as $Y_{\rm L} \equiv n_{\rm L}/s$ with entropy density s. The initial abundance after χ decay $Y_{\rm L}(T_\chi)$ under sudden decay approximation is given by

$$Y_{\rm L}(T_\chi) = \frac{2B(\chi \to 2\text{LSP})}{m_\chi}\left(\frac{\rho_\chi}{s}\right)_{T_\chi} + Y_{\rm L}^{(\rm TP)}, \tag{18}$$

where $B(\chi \to 2\text{LSP})$ is the branching ratio of χ into LSPs and $Y_{\rm L}^{(\rm TP)}$ denotes the contribution from thermal freeze-out, taking into account the dilution from the χ decay. If the annihilation cross section is sufficiently small or the initial abundance of the LSP is negligible, LSPs cannot annihilate each other after χ decays. However, if the annihilation cross section is large enough, the LSP abundance becomes inversely proportional to the annihilation cross section similar to the case of thermal relic abundance,

$$\Omega_{\rm L}h^2 \sim 0.27\left(\frac{10}{g_*(T_\chi)}\right)^{1/2}\left(\frac{100\ \text{MeV}}{T_\chi}\right)\left(\frac{m_{\rm L}}{100\ \text{GeV}}\right) \times \left(\frac{10^{-7}\ \text{GeV}^{-2}}{\langle\sigma v\rangle}\right). \tag{19}$$

The crucial difference is that a larger annihilation cross section is required in order to account for the present dark matter density, because the decay temperature of χ is smaller than the typical freeze-out temperature of the LSP, $T_f \sim m_{\rm L}/20$.

In Fig. 1, the resulting LSP abundance is shown for $m_{\rm L} = 300$ GeV as a function of an annihilation cross section. Dashed (solid) lines correspond to $Y_{\rm L}(T\chi) = 10^{-9}(10^{-11})$ and the left (right) ones correspond to $T\chi = 1(0.1)$ GeV. It is seen that for a large annihilation cross section the result becomes independent of the initial abundance, since the LSP abundance is saturated due to the annihilation effects.

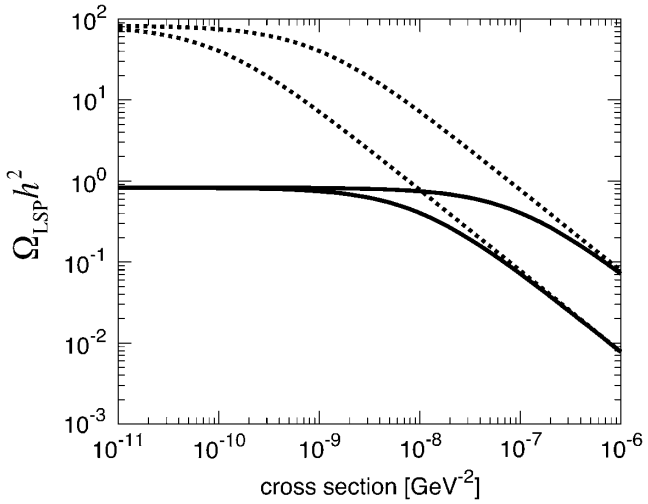

FIG. 1. Nonthermally produced LSP abundance ($\Omega_{\rm LSP}h^2$) as a function of the annihilation cross section ($\langle\sigma v\rangle$). Dashed (solid) lines correspond to $Y_{\rm L}(T\chi) = 10^{-9}(10^{-11})$. Left (right) lines correspond to $T\chi = 1(0.1)$ GeV. Here we have taken $m_{\rm L} = 300$ GeV.

[4]Neutralinos are expected to soon reach kinetic equilibrium due to interactions with background particles in the thermal bath [7,54].

Thus, we are interested in models which predict a large annihilation cross section. For concreteness, we restrict ourselves to two SUSY breaking models: minimal anomaly-mediated SUSY breaking model (MAMSB) and mirage-mediation model (mMSB). The former model predicts the winolike neutralino LSP, which has a naturally large annihilation cross section compared with the case of the binolike neutralino. In the latter model, the annihilation cross section of the binolike neutralino LSP could be enhanced through S-channel resonance, as we will see. Now let us briefly introduce these models.

A. Minimal anomaly-mediation model

In the anomaly-mediated SUSY breaking model, the effect of SUSY breaking in the hidden sector sequestered from the observable sector is transmitted to the MSSM sector through the super-Weyl anomaly effect. Since the SUSY breaking effect is suppressed by a loop factor, the gravitino becomes a few magnitude heavier than the SUSY particles. For example, gaugino masses are given by

$$M_i = b_i \frac{g_i^2}{16\pi^2} m_{3/2}, \tag{20}$$

where g_is are gauge coupling constants for $i = 1$–3 corresponding to $U(1)_Y$, SU(2) and SU(3) gauge groups. The beta function coefficients b_is are calculated as $b_1 = 33/5$, $b_2 = 1$, and $b_3 = -3$. Note that expression (20) is valid for all energy scale μ, not for only the input scale. Thus, it is seen that for weak scale gaugino masses, the gravitino mass can be as heavy as $O(100)$ TeV. One problem of such a scenario is that it predicts tachyonic slepton masses. Thus, in the minimal anomaly-mediation model, an additional universal scalar mass term m_0^2 is introduced to give positive contribution to the scalar masses, as

$$m_{\tilde{f}}^2 = -\frac{1}{4}\left(\frac{d\gamma}{dg}\beta_g + \frac{d\gamma}{df}\beta_f\right) + m_0^2, \tag{21}$$

where β_g and β_f are the beta functions of the corresponding gauge and Yukawa coupling, and $\gamma = \partial \ln Z/\partial \ln \mu$ with Z denoting the wave function renormalization. Therefore this model is characterized by the following parameter set,

$$m_{3/2},\ m_0,\ \tan\beta,\ \mathrm{sign}\,\mu, \tag{22}$$

where $\tan\beta = \langle H_u\rangle/\langle H_d\rangle$ represents the ratio of vacuum expectation values of up-type and down-type Higgses. Here and hereafter, we assume $\mu > 0$ because positive μ is favored from muon $g-2$ experiments.

In this framework the winolike neutralino ($\tilde{W}^0$) naturally becomes the LSP, as is easily seen from Eq. (20). The annihilation process through $\tilde{W}^0\tilde{W}^0 \to W^+W^-$ is not helicity suppressed and hence it has a large annihilation cross section. The annihilation cross section of this process is calculated as [30]

$$\langle \sigma v\rangle = \frac{\pi\alpha_2^2}{2}\frac{m_{\mathrm{L}}^2}{(2m_{\mathrm{L}}^2 - m_W^2)^2}\left(1 - \frac{m_W^2}{m_{\mathrm{L}}^2}\right)^{3/2}, \tag{23}$$

where α_2 is the SU(2) gauge coupling constant and m_W denotes the W-boson mass. Actually, the wino mass should be $\sim$3 TeV to account for the dark matter density if it is produced in the standard thermal freeze-out scenario [55], and such a heavy LSP mass seems to be disfavored from the viewpoint of naturalness. However, if we extend the production mechanism of the LSP to nonthermal origin, the light wino mass of $O(100)$ GeV is favored.

In Fig. 2, we plot the reheating temperature of the χ decay, T_χ, in the $(m_{3/2}, m_0)$ plane with $\tan\beta = 10$, assuming the present dark matter is produced by the decay of the χ field. In most parameter regions, the winolike neutralino LSP is realized with the mass of $\sim m_{3/2}/400$. For larger m_0, the Higgsino mass becomes smaller and the LSP neutralino contains many Higgsino components. Thus, too large values of m_0 are excluded by the absence of electroweak symmetry breaking, and the Higgsino-like LSP is realized near the boundary. As can be seen from this figure, we expect nonthermal production with $0.1\ \mathrm{GeV} < T_\chi < 10\ \mathrm{GeV}$ for the neutralino dark matter with the mass of $\mathcal{O}(100)$ GeV.

B. Mirage-mediation model

The mirage-mediation models are based on recent developments on the moduli-stabilization mechanism in string theory, that is, KKLT construction [33]. We denote the modulus as T and assume the following type of Kähler

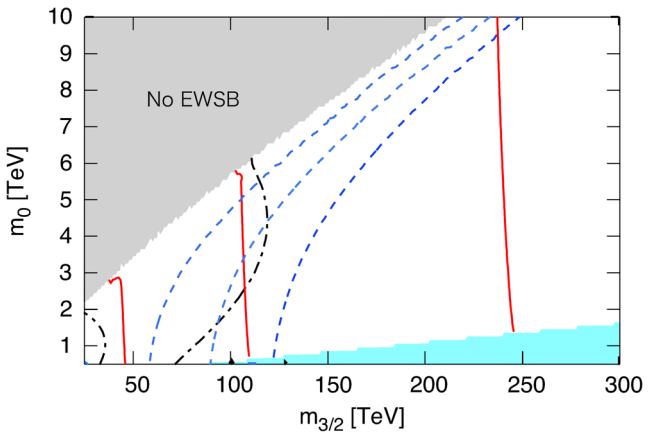

FIG. 2 (color online). Contours of T_χ in order to reproduce correct dark matter abundance and σ_{SI} for the minimal anomaly-mediation model. Red thick solid lines represent $T_\chi = 0.1$, 1, 10 GeV from left to right. Dot-dashed lines show the lightest Higgs mass $m_h = 115$ GeV and 120 GeV and dashed lines correspond to $\mu = 1$, 1.5, 2 TeV from left to right, respectively. The upper left region is excluded from the electroweak symmetry breaking (EWSB) constraint and the lower right region predicts stau LSP or tachyonic slepton masses, and hence is excluded.

potential, superpotential, and gauge kinetic function (hereafter we set $M_P = 1$ unless explicitly written),

$$K = -3\ln(T + T^*) + Z_i(T + T^*)\Phi_i^*\Phi_i, \tag{24}$$

$$W = w_0 - Ae^{-aT} + \frac{\lambda_{ijk}}{6}\Phi_i\Phi_j\Phi_k, \tag{25}$$

$$f_a = kT, \tag{26}$$

where Φ_i denotes MSSM superfields, a and k are real constants, and $Z_i(T + T^*) = 1/(T + T^*)^{n_i}$. The scalar potential for the modulus is given by

$$V_T = e^{K(T+T^*)}[K^{T\bar{T}}|D_T W|^2 - 3|W|^2], \tag{27}$$

where $D_T W = W_T + K_T W$ and $K^{T\bar{T}} = (K_{T\bar{T}})^{-1}$ with the subscript T denoting a field derivative with it. An analysis shows that this potential has a supersymmetric anti-de Sitter minimum. Thus, in order to obtain a de Sitter vacuum consistent with current cosmological observations, the additional uplifting potential is needed. This is provided by, for example, adding an extra brane which is sequestered from the observable brane. The additional term is

$$V_{\rm lift} = \frac{D}{(T + T^*)^m}, \tag{28}$$

where m is $O(1)$ constant. Thus, total scalar potential is given by $V = V_T + V_{\rm lift}$. After fine-tuning the value of D, the desired de Sitter minimum is obtained.

Phenomenologically, this model provides a characteristic pattern of SUSY breaking effect. SUSY is dominantly broken by the uplifting term introduced to make the vacuum energy positive, which becomes a source of anomaly-mediation effect. On the other hand, the modulus T has a nonvanishing F term (F^T) at the resulting vacuum, which becomes a source of modulus-mediation effect. Thus, a mixture of anomaly- and modulus-mediation is realized, called mixed modulus-anomaly mediation [56]. Interestingly, these two effects are comparable in general, that means $F^T/(T + T^*) \sim m_{3/2}/(4\pi^2)$. For example, gaugino masses at the grand unified theory (GUT) scale are given by

$$M_i = C_i\frac{g_i^2}{16\pi^2}m_{3/2} + M_0, \tag{29}$$

where M_0 denotes the modulus-mediation contribution to the gaugino masses at the GUT scale and is calculated as $M_0 = F^T\partial_T \ln{\rm Re}(f_a)$. Taking into account the one-loop renormalization group evolution, gaugino masses at the scale μ are calculated as

$$M_i(\mu) = \frac{g_i^2(\mu)}{g_i^2(M_{\rm mir})}M_0, \tag{30}$$

where the mirage scale $M_{\rm mir}$ is defined as

$$M_{\rm mir} = \frac{M_{\rm GUT}}{(M_P/M_{3/2})^{\alpha/2}}. \tag{31}$$

Here we have defined a parameter α, which characterizes the ratio of the anomaly- to modulus-mediation contribution as

$$\alpha = \frac{m_{3/2}}{M_0\ln(M_P/m_{3/2})}. \tag{32}$$

Thus, all gaugino masses seem to be unified at the mirage scale, which leads to the term of ''mirage-mediation.'' In the original KKLT setup, $\alpha = 1$ is predicted, but α can be regarded as a free parameter in a more general setup. For $\alpha = 1$, the intermediate scale mirage unification ($M_{\rm mir} = 3 \times 10^9$ GeV) is realized. The case of $\alpha = 2$ is called TeV-scale mirage-mediation, since $M_{\rm mir} \sim 1$ TeV is predicted. The tachyonic slepton mass problem in the pure anomaly-mediation model is naturally solved in this framework, because of the modulus-mediation contribution.

Denoting the modulus-mediation contribution to the sfermion masses and A terms at the GUT scale as $\tilde{m}_i^2$ and $\tilde{A}_i$, this model is classified by the following parameters,

$$M_0, c_i, a_i, \tan\beta, \alpha, \tag{33}$$

where we have defined $c_i \equiv \tilde{m}_i^2/M_0^2$ and $a_i \equiv \tilde{A}_i/M_0$, which are related to n_i as $c_i = a_i = 1 - n_i$.

As is obvious from the construction, this model predicts a modulus field T whose mass is estimated as $m_T \sim (8\pi^2)m_{3/2}$. The modulus field is likely to dominate the Universe due to its large energy density stored in the form of scalar condensates with a large initial amplitude of order of the Planck scale. Thus, its decay leads to the nonthermal production of the neutralino dark matter with a reheating temperature of

$$T_T \sim 170\ {\rm MeV}\sqrt{c}\left(\frac{m_T}{10^3\ {\rm TeV}}\right)^{3/2} \tag{34}$$

where we have used the decay rate of the modulus, $\Gamma_T = cm_T^3/4\pi M_P^2$ with $\mathcal{O}(1)$ constant c. In principle, other nonthermal production processes could occur after the modulus decay, and also the nonthermal production with low reheating temperature might be circumvented by the small initial amplitude or heavier modulus mass. Thus, we treat the final reheating temperature T_χ as a free parameter, and pay special attention for the case of $T_\chi < T_T$, which should be satisfied once the modulus field dominates the Universe in the minimal KKLT setup.

Figure 3 shows T_χ in the (M_0, $\tan\beta$) plane with $\alpha = 1$, $c_M = a_M = 1$ for matter fields and $c_H = a_H = 0$ for Higgs fields in the nonthermal production scenario by the χ decay. In these parameter sets, LSP is a binolike neutralino with a mass of $M_1 \simeq (0.4 + 0.3\alpha)M_0$, and its annihilation cross section is enhanced by the s-channel Higgs resonance for $10 < \tan\beta < 20$, and these parameter re-

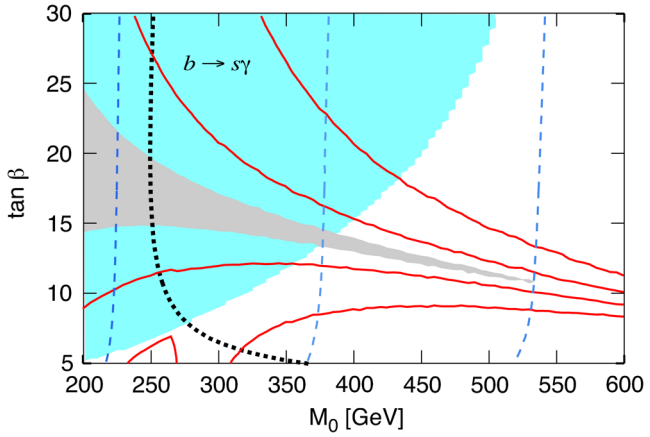

FIG. 3 (color online). Contours of $T_\chi = 10$ GeV and 1 GeV (red thick solid lines) for the mirage-mediation model. The middle gray shaded region corresponds to $T_\chi < T_T$ GeV. The upper left blue shaded region is excluded by the $b \to s\gamma$ constraint. Dotted lines show $m_h = 115$ GeV and dashed lines represent $\mu = 300, 500, 700$ GeV from left to right, respectively.

gions are compatible with the nonthermal production scenario with $T_\chi < 1$ GeV.

III. DETECTION OF NONTHERMAL DARK MATTER

A. Direct detection

Direct detection experiments attempt to observe the recoil energy of a target nucleus scattered elastically by the dark matter. The scattering of a nucleus is discussed in two classes of interactions: spin-dependent (SD) and spin-independent (SI) interactions. For the neutralino dark matter, scattering through spin-independent interactions tends to become important and promising to detect the signals. This scattering mainly occurred by the exchange of Higgs fields and squarks, and the cross section is generally irrelevant to the self-annihilation cross section. Hence, the nonthermal dark matter, which has a large self-annihilation cross section, does not necessarily lead to the enhancement of direct detection signals.

Figures 4 and 5 show the elastic LSP-nucleus SI cross section in anomaly and mirage-mediation models, respectively. Input parameters are chosen randomly with 10 TeV $< m_{3/2} <$ 300 TeV, 0.5 TeV $< m_0 <$ 10 TeV, and $3 < \tan\beta < 50$ for MAMSB, and 200 GeV $< m_{1/2} <$ 600 GeV, $0.5 < \alpha < 2$, $3 < \tan\beta < 50$, and $(c_M, a_M, c_H, a_H) = (1, 1, 1, 1)$, (1,1,0,0), (0.5,0.5,0.5,0.5), (0.5,0.5,0,0) for mMSB. In each parameter set, several phenomenological constraints are imposed, such as the $b \to s\gamma$ constraint, Higgs mass bounds, correct electroweak symmetry breaking condition, and neutralino LSP condition, and the corresponding cross sections are scatter plotted as a function of the LSP mass only for phenomenologically viable parameters. We assume a nonthermal

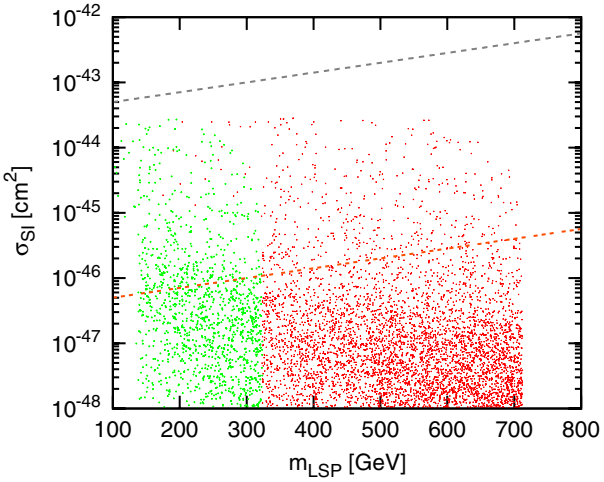

FIG. 4 (color online). Expected SI neutralino-nucleus cross section in MAMSB as a function of the LSP mass. Red (dark) and green (light) points correspond to 1 GeV $< T_\chi <$ 10 GeV and $T_\chi <$ 1 GeV, respectively. The upper dashed line shows the current experimental bound by CDMS, and the lower line represents the future expected sensitivity of the SuperCDMS (stage C).

dark matter production scenario and calculate the appropriate reheating temperature that explains the present dark matter abundance for each parameter. In these figures, the red (dark) and green (light) points correspond to 1 GeV $< T_\chi <$ 10 GeV and $T_\chi <$ 1 GeV, respectively. For the mMSB case, blue (the darkest) points represent the case that the reheating temperature is lower than the modulus decay temperature.

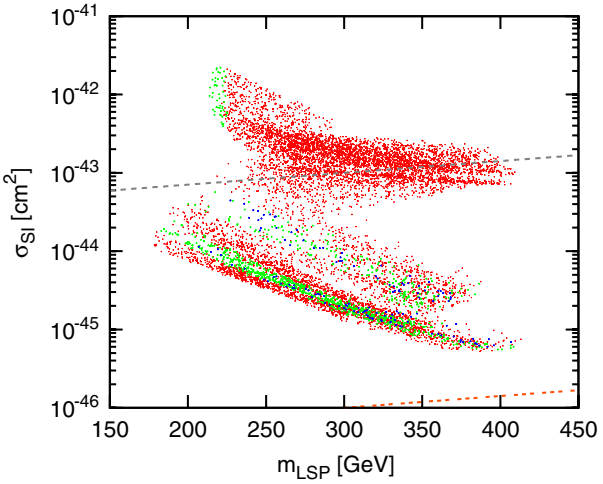

FIG. 5 (color online). Expected SI neutralino-nucleus cross section in mMSB as a function of the LSP mass. Red (dark), green (light), and blue (darkest) dots correspond to 1 GeV $< T_\chi <$ 10 GeV, $T_T < T_\chi <$ 1 GeV, and $T_\chi < T_T$, respectively. Dashed lines are the same as those in Fig. 4.

In the MAMSB model, LSP is a winolike neutralino in almost all parameter regions, and its annihilation cross section is directly correlated with the LSP mass. For example, we need $T_\chi \sim 1$ GeV for $m_{\rm LSP} = 300$ GeV to explain the present dark matter abundance by nonthermal production. On the other hand, the LSP-nucleus scattering amplitude highly depends on the fraction of Higgsino components in the LSP neutralino, which is increased for larger m_0. Hence, the low reheating temperature and LSP-nucleus SI cross section are completely irrelevant as can be seen in Fig. 4.

The same argument can be applied to the mMSB models. In this case, large annihilation cross sections required for the nonthermal dark matter scenario can be realized through s-channel resonance for the binolike neutralino or by the large SU(2) gauge interaction for the Higgsino-like neutralino. However, the annihilation processes are not directly related to the scattering amplitude in both cases, and the predicted LSP-nucleus SI cross section spread in a wide range. In Fig. 5, Higgsino-like neutralinos appear with large SI cross sections around $\sigma_{\rm SI} \simeq 10^{-(42-43)}$ cm^2. This is because mMSB models exhibit rather compressed mass spectrum and the Higgsino-like neutralino has many bino components.

The present strongest upperbounds are given by the CDMS experiment [57] for dark matters with mass of $\mathcal{O}(100)$ GeV and the LSP-nucleus SI cross section must satisfy $\langle\sigma_{\rm SI}\rangle \lesssim 10^{-43}$ cm^2. Thus, the Higgsino-like neutralino produced at $T_\chi < 1$ GeV is disfavored by this bound in the mMSB model. On the contrary, wide parameter regions are allowed both for the binolike neutralino in the mMSB and the winolike neutralino in the MAMSB. They might be explored around $\langle\sigma_{\rm SI}\rangle \gtrsim 10^{-46}$ cm^2 in the projected future sensitivity of the SuperCDMS, stage C. Thus, the possibility to detect the nonthermally produced dark matter by direct detection experiments is highly dependent on the model parameters irrelevant to its production process.

B. Indirect detection

1. Gamma-ray flux from the Galactic center

Observations suggest that the total mass of galaxies are dominated by dark matter. Dark matter forms halo around the galaxy although its density profile still has some uncertainty. We parametrize density profile of the Galactic halo as

$$\rho(r) = \frac{\rho_0}{(\frac{r}{r_0})^a[1 + (\frac{r}{r_0})^b]^{(c-a)/b}}, \tag{35}$$

with r corresponding to the distance from the Galactic center. The Navarro-Frenk-White (NFW) profile [58] corresponds to $a = 1, b = 1, c = 3$, and the isothermal profile corresponds to $a = 0, b = 2, c = 2$. If $a > 0$, the profile shows cuspy structure at the Galactic center and hence the annihilation rate is expected to be enhanced compared to the cored profile.

Neutralino annihilation processes produce both monochromatic and continuum photons, and there are many studies related to this issue [59,60]. The former originates from, e.g., $\tilde\chi\,\tilde\chi \to \gamma\gamma, Z\gamma$, but we have found that branching ratios into these modes are small for interesting parameter regions. Thus, hereafter we concentrate on a continuum gamma-ray flux coming from cascade decays of annihilation products, mainly from pion decays.

Gamma-ray flux produced by the neutralino annihilation at the Galactic center is expressed as [59]

$$\Phi_\gamma(\psi, E) = \frac{\langle\sigma v\rangle}{8\pi m_\chi^2}\frac{dN_\gamma}{dE}\int_{\rm l.o.s.}\rho^2(l)dl(\psi), \tag{36}$$

where the integration is carried out over the line of sight (l.o.s.) and dN_γ/dE represents the differential number of photons with the energy E produced by the neutralino annihilation. This expression shows that the density profile dependent part and particle physics model dependent part can be separated out.

It is convenient to define the dimensionless quantity $J(\psi)$ as

$$J(\psi) = \frac{1}{8.5\ {\rm kpc}}\left(\frac{1}{0.3\ {\rm GeV/cm^3}}\right)^2\int_{\rm l.o.s.}\rho^2(l)dl(\psi), \tag{37}$$

and its averaged value over solid angle $\Delta\Omega$,

$$\langle J\rangle_{\Delta\Omega} = \frac{1}{\Delta\Omega}\int_{\Delta\Omega} d\Omega J(\psi), \tag{38}$$

where $\Delta\Omega = 2\pi(1 - \cos(\psi_{\rm max}))$. In fact, the actual observations have some angular resolution $\Delta\Omega$ and hence the gamma-ray flux from the Galactic center should be integrated over the solid angle. Performing the angular integral, Eq. (36) can be rewritten as

$$\Phi_\gamma(E) \simeq 2.8\times10^{-12}\ {\rm cm^{-2}\,s^{-1}}\frac{dN_\gamma}{dE}\left(\frac{1\ {\rm TeV}}{m_\chi}\right)^2 \times\left(\frac{\langle\sigma v\rangle}{3\times10^{-26}\ {\rm cm^3/s}}\right)\langle J\rangle_{\Delta\Omega}\Delta\Omega. \tag{39}$$

Besides the annihilation cross section and the neutralino mass, the gamma-ray flux crucially depends on the dimensionless quantity $\langle J\rangle_{\Delta\Omega}\Delta\Omega$, which is solely determined by the density profile of the dark matter halo. This is numerically calculated for each profile and solid angle. For the GLAST, $\langle J\rangle_{\Delta\Omega}\Delta\Omega = 3\times10^{-4}$ and 0.1 for the isothermal and NFW profiles, respectively.

In Figs. 6 and 7, the expected integrated gamma-ray fluxes from the Galactic center $\Phi_\gamma(E > 1\ {\rm GeV})$ are shown for MAMSB and mMSB, respectively. Here the isothermal density profile is applied conservatively. The green (light) and red (dark) points correspond to $1\ {\rm GeV} < T_\chi < 10$ GeV and $T_\chi < 1$ GeV, respectively, and the blue (darkest) points are $T_\chi < T_T$. As is apparent from the figures, the

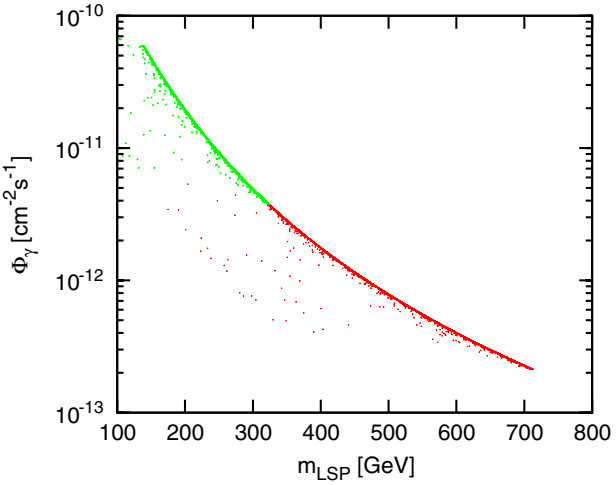

FIG. 6 (color online). Expected gamma-ray flux from the Galactic center above the energy of 1 GeV with the GLAST satellite as a function of the LSP mass in the MAMSB model. The isothermal density profile is assumed.

gamma-ray flux is inversely proportional to the reheating temperature because the same annihilation process is relevant both for the gamma-ray signal and the nonthermal production of the dark matter. Thus, the large annihilation cross section required for nonthermal dark matter directly leads to enhancement of the gamma-ray signal, and its detection possibility becomes increased compared to the case of thermally produced dark matter.

GLAST can detect dark matter annihilation signals if $\Phi_\gamma(E > 1\ \mathrm{GeV}) \gtrsim 10^{-10}\ \mathrm{cm}^{-2}\,\mathrm{s}^{-1}$. Thus, in both cases, it seems difficult to find the gamma-ray signals for the cored profile such as the isothermal one. However, the flux becomes a few orders of magnitude larger for a more cuspy

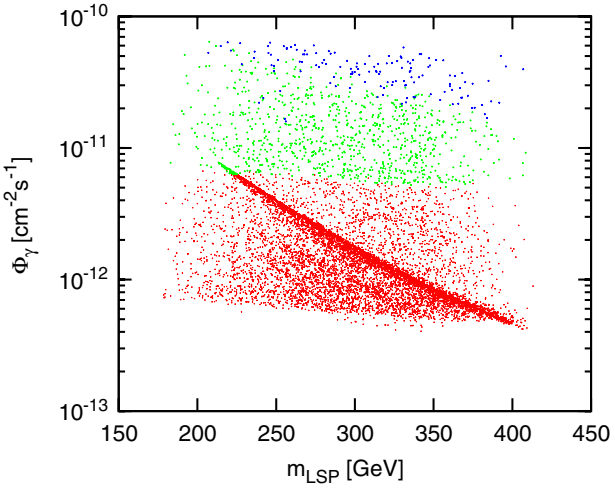

FIG. 7 (color online). Expected gamma-ray flux from the Galactic center above the energy of 1 GeV with the GLAST satellite as a function of the LSP mass in the mMSB model. The isothermal density profile is assumed.

profile, such as the NFW profile, and in that case GLAST may detect dark matter annihilation signals. To summarize, although the definite prediction is impossible due to large uncertainty of the density profile, there is a large possibility to detect the signals from the neutralino dark matter produced nonthermally.

2. Positron flux

Similar to the gamma rays described above, positrons are also yielded by the neutralino annihilation in the Galactic halo. As opposed to the gamma rays, positrons lose their energy through the propagation in interstellar space due to the inverse Compton processes and synchrotron radiation as bent by galactic magnetic fields. For this reason, high-energy positrons can only come from the region within a few kpc around the Earth. Thus, positron flux is insensitive to the density profile of the dark matter halo and implications of its detection on dark matter models are promising [61–63].

Propagations of positrons are described by the following diffusion equation,

$$\frac{\partial}{\partial t} f(E) = K(E)\nabla^2 f(E) + \frac{\partial}{\partial E}[b(E)f(E)] + Q(E), \quad (40)$$

where $f(E)$ denotes the positron number density per unit energy, E denotes the energy of the positron in units of GeV, $K(E)$ is the diffusion constant, $b(E)$ is the energy loss rate, and $Q(E)$ is the source term coming from neutralino annihilation, given as

$$Q(E, \vec{r}) = n_0^2(\vec{r})\langle\sigma v\rangle \frac{d\phi}{dE}, \quad (41)$$

where $d\phi/dE$ denotes the spectrum of the positron from single annihilation. The diffusion constant and energy loss rate are given by [61]

$$K(E) = 3 \times 10^{27}[3^{0.6} + E^{0.6}]\ \mathrm{cm}^2\,\mathrm{s}^{-1}, \quad (42)$$

$$b(E) = 10^{-16}E^2\ \mathrm{s}^{-1}, \quad (43)$$

with E measured in units of GeV. We are interested in a steady state solution, that is, the solution when the left-hand side of Eq. (40) is set to zero. After solving the diffusion equation, the positron flux is given by $\Phi_{e^+}(E) = (c/4\pi)f(E)$ with the speed of light c.

In order to investigate the detection possibility, we define the positron fraction R,

$$R_{e^+}(E) = \frac{\Phi_{e^+}(E)}{\Phi_{e^-}(E) + \Phi_{e^+}(E)}. \quad (44)$$

Here $\Phi_{e^-(e^+)}$ includes background flux coming from the cosmic ray processes. We use the fitting formula for the background positron and electron flux obtained in Refs. [61,64], as

$$\Phi_{e^-}^{(\mathrm{prim})}(E) = \frac{0.16E^{-1.1}}{1 + 11E^{0.9} + 3.2E^{2.15}}, \quad (45)$$

$$\Phi_{e^-}^{(\mathrm{sec})}(E) = \frac{0.70E^{0.7}}{1 + 110E^{1.5} + 600E^{2.9} + 580E^{4.2}}, \quad (46)$$

$$\Phi_{e^+}^{(\mathrm{sec})}(E) = \frac{4.5E^{0.7}}{1 + 650E^{2.3} + 1500E^{4.2}}, \quad (47)$$

in units of $\mathrm{GeV}^{-1}\,\mathrm{cm}^{-2}\,\mathrm{s}^{-1}\,\mathrm{sr}^{-1}$. Superscripts (prim) and (sec) correspond to the primary and secondary origins of them. The reason to use the positron fraction instead of the positron flux itself is that the effect of solar modulation, which is important for the low energy positron flux, is removed by taking the ratio. Another important factor comes from the possible local inhomogeneity for the dark matter distribution in the Galactic halo, characterized by the boost factor (BF), which determines the overall normalization of the positron flux [65]. Here we conservatively assume BF = 1, which means that the homogeneous distribution of the dark matter is assumed.

Figure 8 shows typical positron flux for some model parameters of MAMSB and mMSB. One can see that for the case of MAMSB, the peak signature will be observed. This is because the winolike neutralino mainly annihilates into a W-boson pair and they subsequently decay into e^+, which carry roughly half the energy of the primary W^+ boson. In the case of mMSB where the LSP is mostly binolike, positrons are produced through the cascade decay of the primary annihilation products ($t\bar{t}$), and hence the positron flux accumulates at a rather low energy region. An interesting point is that these dark matters may explain the anomaly reported by the HEAT experiment [66] without introducing any clumpy distribution of the dark matter. To explain this anomaly, a large annihilation cross section of dark matter is required in general, and the nonthermally produced dark matter naturally satisfy it.

The upcoming experiments such as PAMELA and AMS-02 have good sensitivities for a positron energy range 10 GeV $< E <$ 270 GeV. We have performed a χ^2 analysis for investigating detection possibility in these experiments following the method of Ref. [63]. The χ^2 is defined as

$$\chi^2 = \sum_i \frac{(N_i^{\mathrm{obs}} - N_i^{\mathrm{BG}})^2}{N_i^{\mathrm{obs}}}, \quad (48)$$

where N_i^{obs} and N_i^{BG} are the number of positron events and expected background events in the ith energy bin, respectively. We chose 22 energy bins as $\Delta \log E = 0.06$ for $E <$ 40 GeV and $\Delta \log E = 0.066$ for $E > 40$ GeV and assumed a one year operation. Figures 9 and 10 show the resulting χ^2 for PAMELA. The χ^2 for AMS-02 becomes 25 times larger than those for PAMELA. Since a 95% and 99% confidence level correspond to $\chi^2 = 34$ and 40, respectively, PAMELA will surely detect dark matter-originated positron fluxes in a broad parameter region with $T_\chi \lesssim 1$ GeV.

3. Neutrino-induced muon flux from the Sun

Dark matter particles in the halo scatter off the nucleus in the Sun, and then they are trapped and accumulate at the center through the lifetime of the Sun. Trapped neutralinos annihilate with the enhanced rate because of the large number density of the neutralinos in the Sun [67,68]. The neutralino number accumulated in the Sun (N) evolves in a balance between trapped rate and the annihilation rate, as

$$\dot{N} = C_\odot - A_\odot N^2, \quad (49)$$

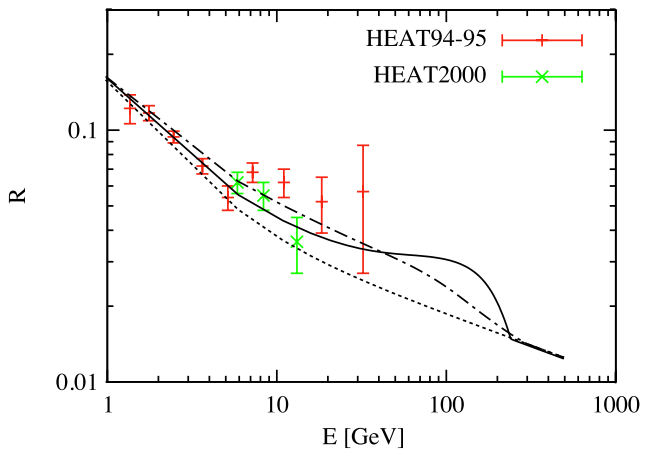

FIG. 8 (color online). Typical positron flux ($R(E)$) as a function of positron energy E (GeV). The solid line corresponds to MAMSB with $m_{3/2} = 80$ TeV and $\tan\beta = 10$, the dot-dashed line corresponds to mMSB with $M_0 = 450$ GeV and $\tan\beta = 13$. The dotted line represents background events.

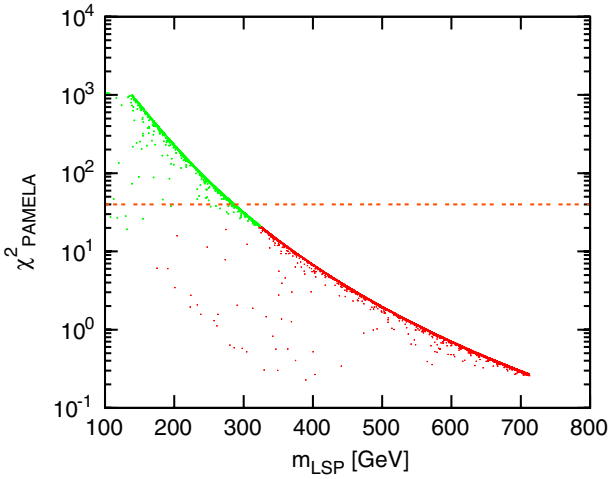

FIG. 9 (color online). Detection possibility of the positron signal by PAMELA in the MAMSB model. We take BF = 1, and 95% and 99% confidence level corresponds to $\chi^2 = 34$, shown by the dashed line, and 40. The definition of each color is the same as Fig. 4.

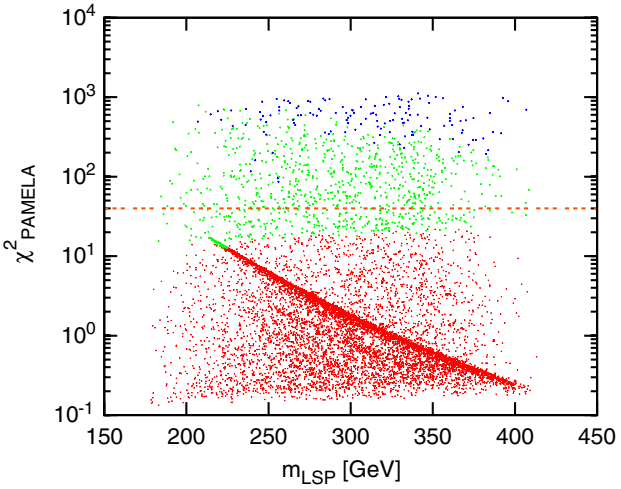

FIG. 10 (color online). Detection possibility of the positron signal by PAMELA in the mMSB model. We take BF = 1, and 95% and 99% confidence level corresponds to $\chi^2 = 34$, shown by the dashed line, and 40. The definition of each color is the same as Fig. 5.

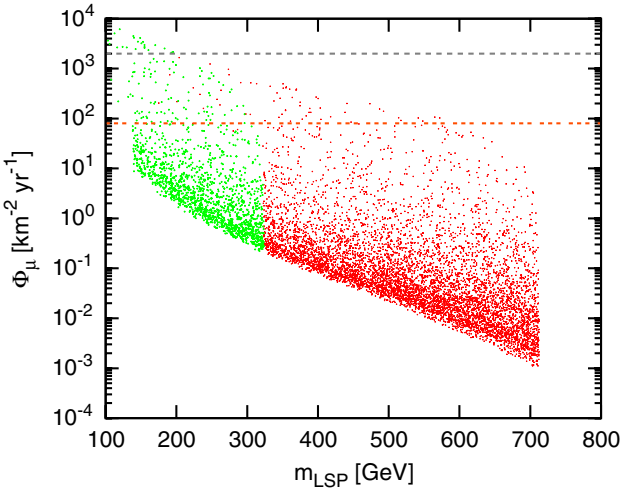

FIG. 11 (color online). Neutrino flux from the Sun in the AMSB model. The upper line shows the current upper bound from Super-K and the lower one shows the sensitivity of IceCube. The definition of each color is the same as Fig. 5.

where $A_\odot \equiv \langle\sigma v\rangle/V$ denotes the annihilation rate with the volume of the Sun, V and $C_\odot$ is the capture rate by the Sun calculated as [1,69]

$$C_\odot \simeq 3.4 \times 10^{20}\ \text{sec}^{-1}\left(\frac{\rho_{\chi\text{solar}}}{0.3\ \text{GeV/cm}^2}\right)\left(\frac{270\ \text{km/s}}{v_{\chi\text{solar}}}\right)^3 \times \left(\frac{\sigma_{\rm H}^{(\rm SD)} + \sigma_{\rm H}^{(\rm SI)} + 0.07\sigma_{\rm He}^{(\rm SI)}}{10^{-42}\ \text{cm}^2}\right)\left(\frac{100\ \text{GeV}}{m_\chi}\right)^2, \quad (50)$$

where $\rho_{\chi\text{solar}}$ and $v_{\chi\text{solar}}$ are local density and velocity of the dark matter around the solar system, $\sigma_{\rm H}$ and $\sigma_{\rm He}$ denote the scattering cross section of the neutralino with hydrogen and helium, respectively, and superscript SD (SI) denote the spin-(in)dependent components of them. These scattering cross sections are limited by the direct detection experiments.

Equation (49) is easily solved analytically and we obtain the annihilation rate Γ as a function of time,

$$\Gamma = \tfrac{1}{2}A_\odot N^2 = \tfrac{1}{2}C_\odot \tanh^2(\sqrt{A_\odot C_\odot}\,t). \quad (51)$$

Thus, we can see that for $\sqrt{A_\odot C_\odot}\,t \gg 1$, which is valid for the case of the Sun ($t_{\rm Sun} \sim 4.5$ Gyr), the annihilation rate is simply given by $\Gamma = C_\odot/2$ and hence independent of the annihilation cross section of the neutralino. Rather, the annihilation rate is determined by the scattering cross section with nucleus. This is because the number density accumulated in the Sun is saturated by the balance between the capture rate and the annihilation rate, and hence the latter is related to the former.

Once neutralinos annihilate in the Sun, energetic neutrinos produced by the subsequent decay of annihilation products escape the Sun and reach to the Earth. They may be observed at the neutrino detectors such as AMANDA and IceCube, which search muon signals resulted from high-energy neutrino-nucleus interactions in the Earth.

In Figs. 11 and 12, the expected neutrino-induced muon fluxes are shown. Here we have taken the threshold energy $E_{\rm th} = 1$ GeV. The muon flux should be restricted below 10^3 km^{-2} yr^{-1} by the current experimental bounds, but almost all of the parameter region is free from this constraint. The expected sensitivity of IceCube is around $\Phi_\mu \simeq 10^2$ km^{-2} yr^{-1} and only the Higgsino-like neutralino in the mMSB model would be promising to be detected. The difference from the gamma ray and positron signals described in the previous subsections is that the high-energy neutrino flux from the Sun is not determined by the annihilation cross section of the neutralino, but by

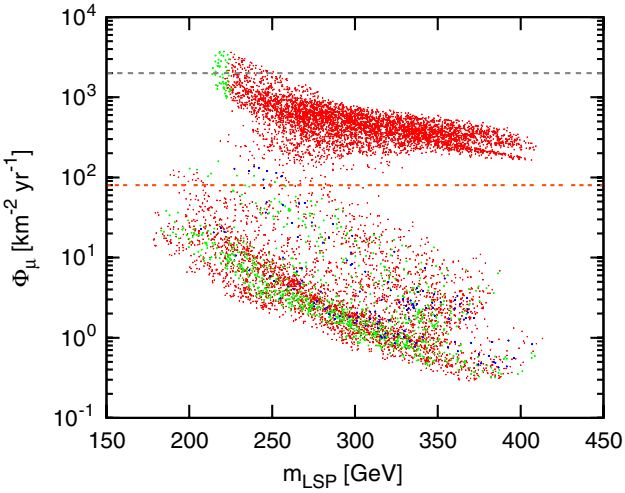

FIG. 12 (color online). Neutrino flux from the Sun in the mMSB model. The upper line shows the current upper bound from Super-K and the lower one shows the sensitivity of IceCube. The definition of each color is the same as Fig. 5.

the scattering cross section of the neutralino with nucleons. Since the scattering cross section is in general not correlated with relic abundance, neutrino-induced muon signals are not so enhanced even if a nonthermal dark matter scenario is assumed.

IV. CONCLUSIONS

We have discussed direct and indirect detection signatures of neutralino dark matters produced nonthermally with a very low reheating temperature $T_d \sim \mathcal{O}(1)$ MeV–$\mathcal{O}(1)$ GeV. In this scenario, the self-annihilation cross section of dark matter should be large enough to account for the present relic abundance. In SUSY models, such a large annihilation cross section is naturally realized for the neutralino dark matter with significant wino or Higgsino components. In the case of the binolike neutralino, such a large annihilation cross section can be obtained by s-channel Higgs resonance. In both cases, the large annihilation cross section leads to the enhancement of gamma-ray signals and the positron flux from the dark matter annihilation, and it becomes promising to detect the nonthermally produced dark matter with $T_\chi \lesssim 1$ GeV by these indirect detection experiments. In other words, the indirect detection experiments may give us clues to explore the history of the Universe with the temperature up to 1 GeV.

Obviously, the consideration with other observations is important and essential to make definitive conclusion about the nonthermal production scenario. For example, it is known that the large annihilation cross section of the LSP affects the BBN, and nonthermally produced dark matter with $T_\chi \lesssim \mathcal{O}(100)$ MeV may be severely constrained by the observation of ^{6}Li abundance [70]. And also the combination with collider experiments may be the most important. The upcoming Large Hadron Collider experiments are expected to discover new particles relevant to the EWSB in the standard model, and there may appear dark matter candidates. Once such a dark matter candidate is discovered, we may have insight on its production mechanism in the Universe by comparing the theoretical calculation of the cross section with cosmological and astrophysical observations, such as the dark matter abundance and its direct and indirect detection signatures. As explained in this paper, large indirect detection signals are characteristic features for the nonthermally produced dark matter, and combined with the Large Hadron Collider experiments we may probe the nature of dark matter by these experiments.

ACKNOWLEDGMENTS

K. N. would like to thank the Japan Society for the Promotion of Science for financial support.

Note added.—While finalizing this manuscript, Ref. [71] was submitted to the preprint server, which studied a similar subject to our present work. While they focus on nonthermally produced wino and higgsinolike dark matter, we have also studied the binolike one in the s-channel resonance region and performed detailed parameter analyses in MAMSB and mMSB models. The main conclusion seems to be consistent with ours.

[1] G. Jungman, M. Kamionkowski, and K. Griest, Phys. Rep. **267**, 195 (1996).
[2] G. Bertone, D. Hooper, and J. Silk, Phys. Rep. **405**, 279 (2005).
[3] E. Komatsu *et al.* (WMAP Collaboration), arXiv:0803.0547.
[4] K. Nakayama, S. Saito, Y. Suwa, and J. Yokoyama, Phys. Rev. D **77**, 124001 (2008); J. Cosmol. Astropart. Phys. 06 (2008) 020.
[5] E. W. Kolb and M. S. Turner, *The Early Universe* (Addison-Wesley, Reading, MA, 1990).
[6] T. Moroi, M. Yamaguchi, and T. Yanagida, Phys. Lett. B **342**, 105 (1995).
[7] M. Kawasaki, T. Moroi, and T. Yanagida, Phys. Lett. B **370**, 52 (1996).
[8] T. A. Perera *et al.*, AIP Conf. Proc. **605**, 485 (2002).
[9] E. Aprile *et al.*, Nucl. Phys. B, Proc. Suppl. **138**, 156 (2005).
[10] http://glast.stanford.edu/.
[11] http://www.mpi-hd.mpg.de/hfm/HESS/HESS.html.
[12] http://magic.mppmu.mpg.de/.
[13] http://www.mpi-hd.mpg.de/hfm/CTA/.
[14] M. S. Longair, *High-Energy Astrophysics* (Cambridge University Press, Cambridge, England, 1994).
[15] M. Boezio *et al.*, Nucl. Phys. B, Proc. Suppl. **134**, 39 (2004).
[16] F. Barao (AMS-02 Collaboration), Nucl. Instrum. Methods Phys. Res., Sect. A **535**, 134 (2004).
[17] S. Desai *et al.* (Super-Kamiokande Collaboration), Phys. Rev. D **70**, 083523 (2004); **70**, 109901(E) (2004).
[18] E. Andres *et al.*, Astropart. Phys. **13**, 1 (2000).
[19] J. Ahrens *et al.* (IceCube Collaboration), Astropart. Phys. **20**, 507 (2004).
[20] http://www.km3net.org/home.php.
[21] L. Randall and R. Sundrum, Nucl. Phys. **B557**, 79 (1999); G. F. Giudice, M. A. Luty, H. Murayama, and R. Rattazzi, J. High Energy Phys. 12 (1998) 027; J. A. Bagger, T. Moroi, and E. Poppitz, J. High Energy Phys. 04 (2000) 009.
[22] K. Choi, A. Falkowski, H. P. Nilles, M. Olechowski, and S. Pokorski, J. High Energy Phys. 11 (2004) 076; K. Choi, A. Falkowski, H. P. Nilles, and M. Olechowski, Nucl. Phys.

B718, 113 (2005).
[23] S. Profumo and P. Ullio, J. Cosmol. Astropart. Phys. 07 (2004) 006.
[24] P. Gondolo, J. Edsjo, P. Ullio, L. Bergstrom, M. Schelke, and E. A. Baltz, J. Cosmol. Astropart. Phys. 07 (2004) 008.
[25] G. B. Gelmini and P. Gondolo, Phys. Rev. D **74**, 023510 (2006); G. Gelmini, P. Gondolo, A. Soldatenko, and C. E. Yaguna, Phys. Rev. D **74**, 083514 (2006).
[26] M. Bolz, A. Brandenburg, and W. Buchmuller, Nucl. Phys. **B606**, 518 (2001); **B790**, 336(E) (2008); J. Pradler and F. D. Steffen, Phys. Rev. D **75**, 023509 (2007); Phys. Lett. B **648**, 224 (2007); V. S. Rychkov and A. Strumia, Phys. Rev. D **75**, 075011 (2007).
[27] L. Roszkowski, R. Ruiz de Austri, and K. Y. Choi, J. High Energy Phys. 08 (2005) 080; D. G. Cerdeno, K. Y. Choi, K. Jedamzik, L. Roszkowski, and R. Ruiz de Austri, J. Cosmol. Astropart. Phys. 06 (2006) 005.
[28] F. D. Steffen, J. Cosmol. Astropart. Phys. 09 (2006) 001.
[29] M. Kawasaki, F. Takahashi, and T. T. Yanagida, Phys. Lett. B **638**, 8 (2006); Phys. Rev. D **74**, 043519 (2006); M. Endo, F. Takahashi, and T. T. Yanagida, Phys. Lett. B **658**, 236 (2008); Phys. Rev. D **76**, 083509 (2007).
[30] T. Moroi and L. Randall, Nucl. Phys. **B570**, 455 (2000).
[31] S. Nakamura and M. Yamaguchi, Phys. Lett. B **655**, 167 (2007).
[32] T. Banks, D. B. Kaplan, and A. E. Nelson, Phys. Rev. D **49**, 779 (1994); B. de Carlos, J. A. Casas, F. Quevedo, and E. Roulet, Phys. Lett. B **318**, 447 (1993).
[33] S. Kachru, R. Kallosh, A. Linde, and S. P. Trivedi, Phys. Rev. D **68**, 046005 (2003).
[34] M. Nagai and K. Nakayama, Phys. Rev. D **76**, 123501 (2007).
[35] M. Hashimoto, K. I. Izawa, M. Yamaguchi, and T. Yanagida, Prog. Theor. Phys. **100**, 395 (1998); K. Kohri, M. Yamaguchi, and J. Yokoyama, Phys. Rev. D **70**, 043522 (2004); **72**, 083510 (2005).
[36] M. Endo, K. Hamaguchi, and F. Takahashi, Phys. Rev. Lett. **96**, 211301 (2006); Phys. Rev. D **74**, 023531 (2006); S. Nakamura and M. Yamaguchi, Phys. Lett. B **638**, 389 (2006); M. Dine, R. Kitano, A. Morisse, and Y. Shirman, Phys. Rev. D **73**, 123518 (2006).
[37] B. S. Acharya, P. Kumar, K. Bobkov, G. Kane, J. Shao, and S. Watson, J. High Energy Phys. 06 (2008) 064.
[38] K. Rajagopal, M. S. Turner, and F. Wilczek, Nucl. Phys. **B358**, 447 (1991).
[39] J. E. Kim, Phys. Rev. Lett. **67**, 3465 (1991); D. H. Lyth, Phys. Rev. D **48**, 4523 (1993); T. Asaka and M. Yamaguchi, Phys. Rev. D **59**, 125003 (1999).
[40] M. Kawasaki, K. Nakayama, and M. Senami, J. Cosmol. Astropart. Phys. 03 (2008) 009.
[41] M. Hashimoto, K. I. Izawa, M. Yamaguchi, and T. Yanagida, Phys. Lett. B **437**, 44 (1998); T. Banks, M. Dine, and M. Graesser, Phys. Rev. D **68**, 075011 (2003); M. Kawasaki and K. Nakayama, Phys. Rev. D **77**, 123524 (2008).
[42] M. Endo and F. Takahashi, Phys. Rev. D **74**, 063502 (2006).
[43] L. Covi, H. B. Kim, J. E. Kim, and L. Roszkowski, J. High Energy Phys. 05 (2001) 033; A. Brandenburg and F. D. Steffen, J. Cosmol. Astropart. Phys. 08 (2004) 008.
[44] K. Y. Choi, J. E. Kim, H. M. Lee, and O. Seto, Phys. Rev. D **77**, 123501 (2008).
[45] S. R. Coleman, Nucl. Phys. **B262**, 263 (1985); **B269**, 744 (E) (1986).
[46] I. Affleck and M. Dine, Nucl. Phys. **B249**, 361 (1985); M. Dine, L. Randall, and S. D. Thomas, Nucl. Phys. **B458**, 291 (1996).
[47] A. Kusenko, Phys. Lett. B **405**, 108 (1997); **404**, 285 (1997); G. R. Dvali, A. Kusenko, and M. E. Shaposhnikov, Phys. Lett. B **417**, 99 (1998); A. Kusenko and M. E. Shaposhnikov, Phys. Lett. B **418**, 46 (1998).
[48] K. Enqvist and J. McDonald, Phys. Lett. B **425**, 309 (1998); Nucl. Phys. **B538**, 321 (1999).
[49] S. Kasuya and M. Kawasaki, Phys. Rev. D **61**, 041301 (2000); **62**, 023512 (2000); **64**, 123515 (2001).
[50] A. G. Cohen, S. R. Coleman, H. Georgi, and A. Manohar, Nucl. Phys. **B272**, 301 (1986).
[51] M. Fujii and K. Hamaguchi, Phys. Lett. B **525**, 143 (2002).
[52] M. Fujii and K. Hamaguchi, Phys. Rev. D **66**, 083501 (2002); M. Fujii and M. Ibe, Phys. Rev. D **69**, 035006 (2004).
[53] M. Fujii and T. Yanagida, Phys. Lett. B **542**, 80 (2002); M. Kawasaki and K. Nakayama, J. Cosmol. Astropart. Phys. 02 (2007) 002; Phys. Rev. D **76**, 043502 (2007).
[54] J. Hisano, K. Kohri, and M. M. Nojiri, Phys. Lett. B **505**, 169 (2001).
[55] J. Hisano, S. Matsumoto, M. Nagai, O. Saito, and M. Senami, Phys. Lett. B **646**, 34 (2007).
[56] K. Choi, K. S. Jeong, and K. i. Okumura, J. High Energy Phys. 09 (2005) 039; M. Endo, M. Yamaguchi, and K. Yoshioka, Phys. Rev. D **72**, 015004 (2005); A. Falkowski, O. Lebedev, and Y. Mambrini, J. High Energy Phys. 11 (2005) 034.
[57] Z. Ahmed *et al.* (CDMS Collaboration), arXiv:0802.3530.
[58] J. F. Navarro, C. S. Frenk, and S. D. M. White, Astrophys. J. **462**, 563 (1996).
[59] L. Bergstrom, P. Ullio, and J. H. Buckley, Astropart. Phys. **9**, 137 (1998).
[60] J. L. Feng, K. T. Matchev, and F. Wilczek, Phys. Rev. D **63**, 045024 (2001); N. W. Evans, F. Ferrer, and S. Sarkar, Phys. Rev. D **69**, 123501 (2004); D. Hooper and L. T. Wang, Phys. Rev. D **69**, 035001 (2004); N. Fornengo, L. Pieri, and S. Scopel, Phys. Rev. D **70**, 103529 (2004); H. Baer, A. Mustafayev, E. K. Park, and S. Profumo, J. High Energy Phys. 07 (2005) 046; S. Profumo, Phys. Rev. D **72**, 103521 (2005); F. Ferrer, L. M. Krauss, and S. Profumo, Phys. Rev. D **74**, 115007 (2006); G. Zaharijas and D. Hooper, Phys. Rev. D **73**, 103501 (2006); S. Dodelson, D. Hooper, and P. D. Serpico, Phys. Rev. D **77**, 063512 (2008); S. Profumo, Phys. Rev. D **78**, 023507 (2008).
[61] E. A. Baltz and J. Edsjo, Phys. Rev. D **59**, 023511 (1998).
[62] E. A. Baltz, J. Edsjo, K. Freese, and P. Gondolo, Phys. Rev. D **65**, 063511 (2002); G. L. Kane, L. T. Wang, and J. D. Wells, Phys. Rev. D **65**, 057701 (2002); Y. Mambrini and C. Munoz, J. Cosmol. Astropart. Phys. 10 (2004) 003; J. Hisano, S. Matsumoto, O. Saito, and M. Senami, Phys. Rev. D **73**, 055004 (2006).
[63] D. Hooper and J. Silk, Phys. Rev. D **71**, 083503 (2005).
[64] I. V. Moskalenko and A. W. Strong, Astrophys. J. **493**, 694 (1998).
[65] J. Silk and A. Stebbins, Astrophys. J. **411**, 439 (1993); L. Bergstrom, J. Edsjo, P. Gondolo, and P. Ullio, Phys. Rev.

D **59**, 043506 (1999).
[66] S. W. Barwick *et al.* (HEAT Collaboration), Astrophys. J. **482**, L191 (1997); J. J. Beatty *et al.*, Phys. Rev. Lett. **93**, 241102 (2004).
[67] S. Ritz and D. Seckel, Nucl. Phys. **B304**, 877 (1988).
[68] M. Kamionkowski, Phys. Rev. D **44**, 3021 (1991); G. Jungman and M. Kamionkowski, Phys. Rev. D **51**, 328 (1995); L. Bergstrom, J. Edsjo, and P. Gondolo, Phys. Rev. D **55**, 1765 (1997); **58**, 103519 (1998); V. D. Barger, F. Halzen, D. Hooper, and C. Kao, Phys. Rev. D **65**, 075022 (2002); F. Halzen and D. Hooper, Phys. Rev. D **73**, 123507 (2006); J. Liu, P. f. Yin, and S. h. Zhu, Phys. Rev. D **77**, 115014 (2008).
[69] A. Gould, Astrophys. J. **388**, 338 (1992).
[70] K. Jedamzik, Phys. Rev. D **70**, 083510 (2004).
[71] P. Grajek, G. Kane, D. J. Phalen, A. Pierce, and S. Watson, arXiv:0807.1508.